Research Square

Preprints are preliminary reports that have not undergone peer review.
They should not be considered conclusive, used to inform clinical practice,
or referenced by the media as validated information.

Cerebellar functional reorganization across mandibular positions in painful temporomandibular disorder: an fMRI case report integrated with cerebellar voxel-based morphometry

Nataliia Savychuk
Shupyk National Healthcare University of Ukraine
Vasil Pekhno
Pekhnyo@ukr.net

Shupyk National Healthcare University of Ukraine
Ivan Riabko
Taras Shevchenko National University of Kyiv

Case Report

Keywords: Temporomandibular disorders, cerebellum, functional magnetic resonance imaging, voxel-based morphometry, SUIT atlas

Posted Date: April 23rd, 2026

DOI: https://doi.org/10.21203/rs.3.rs-9177677/v1

License: This work is licensed under a Creative Commons Attribution 4.0 International License. Read Full License

Additional Declarations: No competing interests reported.

Abstract

Background

Painful temporomandibular disorder is common, but cerebellar responses to different mandibular states remain insufficiently described. This case is reported because it shows a novel within-subject pattern of state-dependent cerebellar blood oxygen level-dependent signal redistribution.

Case presentation:

A 27-year-old woman presented with persistent jaw tension, bruxism, and subjective chronic tinnitus of approximately 2 years duration. Brain magnetic resonance imaging with task-based functional imaging was performed using a block-design rest-task paradigm. During imaging, the patient performed jaw-closing tasks under three experimentally defined mandibular conditions: centric occlusion, a splint condition, and centric relation. Functional data were preprocessed in standard space and analyzed using voxelwise and region-of-interest-based cerebellar assessment with the SUIT Nettekoven Asym32 atlas. The splint condition showed the largest number of cerebellar clusters and the broadest topographic distribution, but these activations were mainly small and spatially fragmented. Centric relation showed the largest total activated volume and the highest peak signal, consistent with more consolidated activation fields. Centric occlusion showed fewer clusters overall but the highest mean signal intensity. Model-based analysis did not identify a robust global main effect of mandibular condition; however, region-specific effects and an interaction between cerebellar region and centric relation suggested condition-dependent redistribution of cerebellar activity.

Conclusions

This case demonstrates that cerebellar blood oxygen level-dependent responses in painful temporomandibular disorder may vary according to mandibular state in a region-specific manner. The findings provide pathophysiological insight into cerebellar involvement in temporomandibular disorder and suggest potential value for individualized functional assessment in complex cases.

Background

Temporomandibular disorders (TMD) are musculoskeletal pain conditions involving the temporomandibular joint and/or the masticatory muscles. They are among the most common chronic musculoskeletal disorders, affecting an estimated 6–12% of the general population. Despite their high prevalence, management remains largely multimodal rather than mechanism-specific. Pain is one of the main reasons patients seek care, and reported average pain intensity in TMD has been shown to be comparable to that of other clinically significant pain conditions, including chest and back pain [1].

The cerebellum plays an important role in motor coordination while integrating diverse sensory inputs [2]. Human neuroimaging studies have consistently demonstrated cerebellar involvement in both physiological and pathological pain states [3–7]. In TMD, a limited number of neuroimaging studies have reported

cerebellar activation, including findings in the left cerebellar hemisphere [8, 9]. In addition, several studies suggest that central nervous system activity may vary according to mandibular position or occlusal state, which is consistent with the cerebellum's role in sensorimotor integration and adaptive motor control [10–13].

To our knowledge, no case-based functional magnetic resonance imaging (fMRI) report has described within-subject cerebellar BOLD signal redistribution across different mandibular positions in TMD. This case may therefore provide a novel pathophysiological perspective and potential diagnostic insight into state-dependent brain responses in TMD.

Case presentation

This case was evaluated within a study protocol approved by the Commission on Ethics and Academic Integrity of the Shupyk National Healthcare University of Ukraine (Protocol No. 13/10; Ukrainian Research Registration No. 0125U003930). Written informed consent for clinical and imaging assessment was obtained from the patient before participation.

A 27-year old female presented to the Department of Therapeutic and Pediatric Dentistry and Department of Orthopedic Dentistry, Digital Technologies and Implantology, Faculty of Dentistry, Shupyk National Healthcare University of Ukraine, on October 22, 2024. The main complaints were persistent jaw tension, bruxism, and subjective chronic tinnitus that had been present for approximately 2 years.

Clinical findings

On clinical examination, the patient reported pain on palpation of the left temporalis muscle, left lateral pterygoid muscle, and left temporomandibular joint region. She also reported left-sided otalgia and pain radiating to the left periauricular region. Maximum mouth opening was 43 mm, with deviation to the left during opening. Joint clicking was present in the left temporomandibular joint. No neurological abnormalities were observed. These findings were considered consistent with a painful temporomandibular disorder phenotype.

Diagnostic assessment

Based on the clinical presentation, palpation findings, mandibular deviation during opening, joint clicking, and imaging work-up, the case was classified as painful temporomandibular disorder. Structural MRI was used to assess the anatomical context, whereas task-based fMRI was used to investigate condition-dependent cerebellar functional responses across different mandibular states.

Outcome and follow-up

No adverse events related to the imaging procedure were observed. The case was primarily investigated for diagnostic and pathophysiological characterization rather than for assessment of treatment efficacy. At

the time of reporting, the patient remained under clinical observation, and the present report focuses on the imaging phenotype observed during the study protocol.

Patient perspective:

The patient reported that the most disturbing symptoms were persistent jaw tension and chronic tinnitus, both of which she considered clinically meaningful in everyday life. She perceived the imaging-based assessment as important because it could help clarify whether different mandibular positions were associated with different symptom-related brain responses.

Timeline

Symptoms of persistent jaw tension, bruxism, and subjective chronic tinnitus had been present for approximately 2 years before the patient sought specialist evaluation. She presented on October 22, 2024, to the Faculty of Dentistry of Shupyk National Healthcare University of Ukraine for clinical assessment. Following informed consent, structural MRI and task-based fMRI were performed at the National Children's Specialized Hospital "Okhmatdyt."

Magnetic resonance imaging was performed at the Radiology Department of the National Children's Specialized Hospital "Okhmatdyt," Ministry of Health of Ukraine. Brain functional MRI was acquired using a block-design rest-task paradigm. During imaging, the patient performed jaw-closing tasks under three experimentally defined mandibular conditions: centric occlusion (CO), a splint condition, and centric relation (CR). These conditions were used as comparative functional states during imaging rather than as treatment outcomes.

Functional activation maps were superimposed on anatomical T1-weighted brain MRI images. Functional data were preprocessed and co-registered to MNI152 space. Imaging parameters were as follows: repetition time 4000 ms, echo time 97 ms, slice thickness 5.0 mm, 25 slices, distance factor 30%, field of view 230 mm, phase field of view 100%, base resolution 128, phase resolution 100%, GRAPPA acceleration factor 2, reference lines 32, partial Fourier 6/8, distortion correction off, raw filter on, elliptical filter off, strong fat saturation, standard dynamic mode, magnitude reconstruction, and AutoAlign (Head > Brain).

To characterize state-dependent cerebellar responses across mandibular conditions, both voxelwise and ROI-based analyses were performed. Voxelwise analysis was conducted in FEAT (FSL v6.0.7.18) using a general linear model to generate Z-statistic maps, with a threshold of $Z > 3.1$ and cluster-wise correction at $p < 0.05$ based on Gaussian random field theory. ROI-level cerebellar characterization was performed using the SUIT Nettekoven Asym32 atlas [14], selected because of its multimodal organization and sufficiently detailed cerebellar parcellation. For each mandibular condition, the activation index, voxel counts, peak uncorrected p-values, and FRD were calculated for activated cerebellar regions.

To compare cerebellar response profiles across CO, splint condition, and CR, pairwise contrasts between conditions were also examined. Pattern similarity across conditions was further explored using cosine

similarity, Euclidean distance, and mean absolute difference. Hierarchical clustering and consensus heatmaps were used to evaluate ROI-level organization across mandibular states. Structural cerebellar morphometric assessment was performed on anatomical MRI using FreeSurfer (v7.4.1). HOROS (v3.3.6) was used for MRI visualization, and MATLAB (R2024a) was used for statistical processing.

Imaging findings

As summarized in Table 1, cerebellar activation varied across the three mandibular conditions, predominantly through ROI-specific redistribution rather than a uniform global shift. The splint condition showed the largest number of clusters (21) and the widest topographic distribution, involving 13 unique ROIs. However, this pattern was predominantly fragmented, with a median cluster size of 30 voxels, a mean cluster size of 578 voxels, a mean Z-statistic of 4.251, and a maximum Z-statistic of 6.023. Thus, under the splint condition, activation was distributed across a larger number of small and spatially fragmented cerebellar clusters.

Table 1
General fMRI results across all conditions

Mandibular position	Number of clusters	Number of voxels	Cluster size		Z-statistic		Unique ROIs in rows
			median	mean	mean	max	
CO	8	11 646	523	1455,75	5.065	6.898	8
Splint condition	21	12 157	30	578	4,251	6.023	13
CR	11	15 495	85	1408.63	4.809	7.398	8

The CR condition showed a distinct pattern. Although fewer clusters were identified (11), the total activated volume was the largest (15,495 voxels), with a mean cluster size of 1408.63 voxels, a median cluster size of 85 voxels, and the highest peak response in the dataset (Zmax = 7.398). This pattern was associated with more spatially consolidated activation fields and higher peak intensity in selected ROIs.

CO showed an intermediate spatial pattern, with 8 clusters and a total activated volume of 11,646 voxels, but it had the highest mean Z-statistic (5.065; Zmax = 6.898). Compared with the splint condition, activation under CO was less spatially dispersed but relatively more intense at the voxel level, with larger clusters overall (median 523 voxels; mean 1455.75 voxels).

Detailed ROI-level findings, including anatomical region, cluster overlap, activation index, voxel count, uncorrected peak p-values, FRD, and SUIT coordinates, are presented in Table 2.

Table 2
The results of preprocessing the data according to SUIT Nettekoven Asym32 atlas

Anato-mical region		Over-lap in cluster (%)	Other regions (label: share%)	Activa-tion index (peak Z/T)	Number of voxels in cluster	Uncorr. p (peak)	FDR q (peaks)	SUIT coords NMI152 (x y z)		
Centric occlusion										
1.	D2R	24.1	S4R:22.3%; S2R:18.2%	6,898	4379	5,27E-12	4,22E-11	35	-39	-41
2.	S1L	24.8	D1L:12.8%; D3L:11.3%	6,403	4677	1,52E-10	6,1E-10	29	-56	34
3.	S1L	42.2	S2L:33.9%; D1L:12.3%	6,048	495	1,47E-09	3,91E-09	40	-83	3
4.	S2R	58.0	D2R:19.2%; S3R:7.1%	5,682	1484	1,33E-08	2,66E-08	24	-83	-28
5.	M3R	36.9	S1R:32.5%; D4R:11.8%	4,577	550	4,71E-06	7,54E-06	35	-63	-16
6.	A2R	60.0	M4R:16.4%; S5R:10.9%	4,396	55	1,1E-05	1,47E-05	40	-52	-20
7.	D2R	60.0	D3R:40.0%	3,406	5	0,000659	0,000753	28	v	-31
8.	S2R	100.0		3,106	1	0,001896	0,001896	40	-54	-15
Splint condition										
1.	D3L	21.5	S2L:19.5%; S1L:17.8%	6,023	5416	1,71E-09	3,59E-08	29	-57	36
2.	D2R	48.2	S4R:32.6%; S2R:12.6%	5,837	709	5,31E-09	5,57E-08	43	-44	-49
3.	D1R	43.6	S1R:31.6%; M1R:12.6%	5,646	427	1,64E-08	1,15E-07	26	-69	-20
4.	D3R	55.4	D2R:34.7%; D1R:6.4%	5,204	623	1,95E-07	1,02E-06	46	-69	-29
5.	M2L	23.5	M3L:22.1%; D3L:21.9%	5,031	2204	4,87E-07	2,04E-06	9	-44	-3
6.	D2R	52.2	S4R:34.1%; S2R:11.2%	4,821	1251	1,43E-06	4,77E-06	46	-59	-49
7.	D2R	72.3	D4R:27.7%	4,799	47	1,59E-06	4,77E-06	31	-60	-37
8.	M3L	60.4	M4L:36.7%; D2L:2.1%	4,742	283	2,12E-06	5,56E-06	18	-38	4
9.	S2R	64.4	S1R:20.3%; S4R:12.3%	4,475	1061	7,64E-06	1,78E-05	26	-82	-27

Anato-mical region		Over-lap in cluster (%)	Other regions (label: share%)	Activa-tion index (peak Z/T)	Number of voxels in cluster	Uncorr. p (peak)	FDR q (peaks)	SUIT coords NMI152 (x y z)		
Centric occlusion										
10.	S1L	60.0	S2L:40.0%	4,315	20	1,59E-05	3,35E-05	33	-67	19
11.	M3R	100.0		4,051	42	5,1E-05	9,74E-05	41	-55	-29
12.	D3R	100.0		3,969	8	7,23E-05	0,000127	29	-54	-33
13.	M2R	76.7	D3R:16.7%; D2R:6.7%	3,755	30	0,000174	0,00028	24	-57	-26
14.	M3L	87.5	M2L:12.5%	3,623	16	0,000291	0,000437	39	-58	10
15.	M2R	100.0		3,547	4	0,000389	0,000545	22	-58	-10
16.	D3R	100.0		3,44	6	0,000583	0,000737	23	-59	-52
17.	A1R	100.0		3,433	3	0,000597	0,000737	42	-38	-40
18.	M1R	100.0		3,169	2	0,001527	0,001722	11	-74	-16
19.	D1R	100.0		3,164	3	0,001558	0,001722	15	-83	-20
20.	S1L	100.0		3,117	1	0,001829	0,001864	31	-72	6
21.	M2R	100.0		3,111	1	0,001864	0,001864	25	-61	-10
Centric Relation										
1.	S2R	47.1	D2R:21.4%; S4R:21.3%	7,398	4503	1,38E-13	1,52E-12	33	-52	-45
2.	S1L	13.5	M2L:11.3%; D1L:10.0%	6,254	9086	4E-10	2,2E-09	1	-52	-5
3.	D3L	45.7	D2L:36.9%; D4L:10.4%	5,755	833	8,64E-09	3,17E-08	29	-54	31
4.	M4R	30.0	S5R:28.8%; S2R:11.6%	5,379	604	7,49E-08	2,06E-07	40	-49	-16
5.	S1R	46.4	M3R:19.3 D3R:15.0%	5,032	274	4,84E-07	1,07E-06	36	-56	-16
6.	D3R	31.8	A1R:31.8%; M2R:18.8%	4,801	85	1,58E-06	2,89E-06	51	-50	-42
7.	M4L	89.7	D2L:5.1%; A2L:5.1%	4,049	39	5,15E-05	8,09E-05	15	-38	4
8.	M4R	100.0		3,987	37	6,69E-05	9,2E-05	24	-36	-25
9.	S1R	100.0		3,643	25	0,000269	0,000329	33	-70	-30

Anato-mical region		Over-lap in cluster (%)	Other regions (label: share%)	Activa-tion index (peak Z/T)	Number of voxels in cluster	Uncorr. p (peak)	FDR q (peaks)	SUIT coords NMI152 (x y z)		
Centric occlusion										
10.	A3R	100.0		3,349	6	0,000811	0,000893	48	-44	-39
11.	M3R	100.0		3,249	3	0,001158	0,001158	11	-52	-21

At the model level, generalized linear modeling did not identify a significant global main effect of mandibular condition on the activation index. In the condition-only model, neither CR nor the splint condition differed significantly from CO (all $p > 0.5$), and the overall F-test was not significant ($p = 0.862$). When ROI was added in the model, the ROI effect was significant ($p = 0.019$), whereas the condition effect remained non-significant. An ROI × condition interaction was observed for CR ($p = 0.042$), indicating that the relationship between activation index and ROI differed between CR and CO, although the overall model showed only borderline significance ($F = 2.39$, $p = 0.068$).

For voxel count, the condition-only model also showed no global between-state differences (all $p > 0.6$). ROI remained significant in models including ROI ($p = 0.011$) and ROI × condition interaction terms ($p = 0.028$). A weak interaction signal was observed for the splint condition by ROI ($p = 0.093$), suggesting that the spatial distribution of cluster size may differ across ROIs under this condition, although no robust global state effect was detected.

For false discovery rate-adjusted q-values (FRD), the splint condition showed only a trend toward higher values compared with CO ($p = 0.107$ in the condition-only model; $p = 0.105$ after inclusion of ROI; $p = 0.059$ in the interaction model), without reaching conventional statistical significance. Uncorrected p-values did not show systematic differences across states or ROIs in any of the tested models. Taken together, these analyses suggest that local ROI-specific changes were more prominent than global average shifts across mandibular conditions.

Figure 1 illustrates the top 10 cerebellar ROIs across CO, the splint condition, and CR. Across all panels, the dominant pattern was not a uniform increase or decrease in signal, but rather a redistribution of activation among specific cerebellar regions. The highest activation index in S1L was observed under CR, with lower values under CO and the splint condition. In contrast, D2R and S2R were most prominent under CO, whereas D3L and M2L showed their highest activation under the splint condition. M3R, A2R, D3R, M4R, and S1R showed more moderate values without a single consistently dominant condition.

The voxel-count profiles also varied by ROI. S1L showed its largest cluster under CR, with intermediate values under CO and minimal representation under the splint condition. D2R and S2R showed their largest clusters under CO, whereas D3L and M2L were most pronounced under the splint condition (Fig. 2). These findings support the interpretation that mandibular state was associated with ROI-specific redistribution of cerebellar activation rather than a consistent global increase or decrease.

Pairwise comparisons between conditions further supported this regional patterning. CO was characterized by stronger right-sided involvement of D2R, S2R, and A2R. The splint condition shifted the dominant response toward left-sided D3L and M2L, whereas CR was associated with more consolidated activation in S1L and was additionally associated with right-sided S1R and M4R. Most of the strongest peaks remained significant after FDR correction. According to the ROI comparison analysis (Table 3), the main between-condition differences were therefore regional rather than global.

Table 3
ROI comparison analysis

ROI	Metric	CO-CR	CO-Splint condition	CR-Splint condition
S1L	AI	0,149	3,286	3,137
D2R	AI	5,27	-0,567	-5,837
S2R	AI	-1,716	1,207	2,923
M3R	AI	4,577	0,526	-4,051
A2R	AI	4,396	4,396	0
D3L	AI	-5,755	-6,023	-0,268
M2L	AI	0	-5,031	-5,031
D3R	AI	0	-4,742	-4,742
M4R	AI	-5,379	0	5,379
S1R	AI	-5,032	0	5,032
S1L	Vx	-4409	4657	9066
D2R	Vx	4379	3670	-709
S2R	Vx	-3019	423	3442
M3R	Vx	550	508	-42
A2R	Vx	55	55	0
D3L	Vx	-833	-5416	-4583
M2L	Vx	0	-2204	-2204
D3R	Vx	0	-637	-637
M4R	Vx	-604	0	604
S1R	Vx	-299	0	299
S1L	p	-2,48E-10	-1,58998E-05	-1,58996E-05
D2R	p	5,27E-12	-5,30473E-09	-5,31E-09
S2R	p	1,32999E-08	-7,6267E-06	-7,64E-06
M3R	p	0,00000471	-0,00004629	-0,000051
A2R	p	0,000011	0,000011	0
D3L	p	-8,64E-09	-1,71E-09	6,93E-09
M2L	p	0	-0,000000487	-0,000000487

ROI	Metric	CO-CR	CO-Splint condition	CR-Splint condition
D3R	p	0	-0,00000212	-0,00000212
M4R	p	-7,49E-08	0	7,49E-08
S1R	p	-0,000000484	0	0,000000484
S1L	FDR	-1,59E-09	-3,34994E-05	-3,34978E-05
D2R	FDR	4,22E-11	-5,56578E-08	-5,57E-08
S2R	FDR	2,65985E-08	-1,77734E-05	-1,78E-05
M3R	FDR	0,00000754	-0,00008986	-0,0000974
A2R	FDR	0,0000147	0,0000147	0
D3L	FDR	-3,17E-08	-3,59E-08	-4,2E-09
M2L	FDR	0	-0,00000204	-0,00000204
D3R	FDR	0	-0,00000556	-0,00000556
M4R	FDR	-0,000000206	0	0,000000206
S1R	FDR	-0,00000107	0	0,00000107

Additional analyses of ROI appearance and disappearance relative to CO are summarized in Table 4, and hierarchical clustering with consensus heatmaps is presented in Table 5. ROI labels were grouped into motor (M), action/attention (A), multi-demand/default-mode (D), and speech/semantic (S) territories. Under CO, clustering emphasized right-sided S2R and D2R together with stable A2R/M3R involvement. Under the splint condition, left-sided D3L and M2L became more distinctive, consistent with broader but less consolidated recruitment. Under CR, the clustering structure appeared more stable, with strong segregation of S1L, S2R, M4R, and S1R. Overall, these exploratory analyses reinforced the interpretation that mandibular state was associated with ROI-specific cerebellar redistribution rather than a uniform global shift.

Table 4
ROI appearance and disappearance relative to CO

Splint condition vs CO:	**Appeared in the Splint condition (absent in CO)**	**Disappeared in the Splint condition (present in CO)**
	D3L, M2L, D3R	**A2R**
	Present in both	
	S1L, D2R, S2R, M3R	
CR vs CO	Appeared in CR (absent in CO)	Disappeared in CR (present in CO)
	S1R, M4R, D3L	S1R, M4R, D3L
	Present in both	
	S1L, S2R	

Table 5
ROI clusters for activated ROI Ai, FDR, p-value, Voxels

Voxels	FDR q	p-value	Activation Index
CO **(mean s = 0.88):** **C1: S2R;** **C2: M3R, A2R, D3L, M2L, D3R, M4R, S1R;** **C3: S1L, D2R**	**CO** **(mean s = 1.00)** **C1: M3R;** **C2: A2R;** **C3: S1L, D2R, S2R, D3L, M2L, D3R, M4R, S1R.**	**CO** **(mean s = 1.00):** **The same as CO FDR q**	**CO** **(mean s = 0.78):** **C1: M3R, A2R;** **C2: S1L, D2R, S2R; C3: D3L, M2L, D3R, M4R, S1R.**
Splint condition **(mean s = 0.77)**: C1: M2L; C2: S1L, D2R, S2R, M3R, A2R, D3R, M4R, S1R; C3: D3L.	**Splint condition** **(mean s = 0.80)** C1: D2R, A2R, D3L, M2L, D3R, M4R, S1R; C2: S1L, S2R; C3: M3R	The same as Splint condition FDR q	**Splint condition** **(mean s = 0.68)**: C1: D2R, D3L; C2: S1L, S2R, M3R, M2L, D3R; C3: A2R, M4R, S1R.
CR **(mean s = 0.93)**: C1: S1L; C2: S2R; C3: D2R, M3R, A2R, D3L, M2L, D3R, M4R, S1R.	**CR** **(mean s = 0.96)** C1: M4R; C2: S1L, D2R, S2R, M3R, A2R, D3L, M2L, D3R; C3: S1R.	**CR** **(mean s = 0.97)** C1: M4R; C2: S1L, D2R, S2R, M3R, A2R, D3L, M2L, D3R; C3: S1R.	**CR** **(mean s = 0.83)**: C1: S2R; C2: S1L, D3L, M4R, S1R; C3: D2R, M3R, A2R, M2L, D3R.

Discussion and conclusions

Systematic reviews have shown that TMD is associated not only with abnormalities in the trigemino-thalamo-cortical system, but also with alterations in the lateral and medial pain systems, the default mode network, the descending antinociceptive periaqueductal gray-raphe magnus pathway, and motor-related circuits. At the same time, both reviews emphasized substantial methodological heterogeneity, which has limited cross-study comparability and made it difficult to define a single canonical neuroimaging phenotype for TMD [15, 16].

Recent studies further support the view that TMD is characterized by distributed brain changes rather by than single uniform biomarker. In a 2025 pilot whole-brain voxel-based analysis, patients with TMD showed increased gray matter volume in several frontal, sensorimotor, and temporal regions, while cerebral perfusion changes were more restricted, with significantly higher cerebral blood flow identified only in the

medial segment right postcentral gyrus; importantly, pain intensity, anxiety, depression, and jaw functional limitation were differentially associated with these morphometric and perfusion findings. In parallel, a 2026 resting-state fMRI graph-theory study reported reduced clustering coefficient and local efficiency in TMD, with local efficiency correlating positively with depressive and anxious symptoms. Together, these findings suggest that TMD involves maladaptive plasticity at both structural and network levels, whereas the cerebellum has remained relatively underemphasized in most recent studies [17, 18].

Against this background, the present case adds a distinct perspective by focusing specifically on the cerebellum and by examining cerebellar responses within the same patient across different mandibular states. This is relevant because contemporary pain literature increasingly recognizes the cerebellum as more than a motor structure. A 2024 review argued that lobules IV-VI and Crus I are particulary relevant to pain processing and that the cerebellum likely modulates pain through its communication with sensorimotor, executive, reward, and limbic systems. A 2025 narrative review further highlighted recurrent involvement of Crus I, lobules VI and VIII, and the vermis across chronic pain conditions, including migraine and chronic low back pain, with implications for both sensory-discriminative and affective-motivational dimensions of pain. Within such a framework, cerebellar BOLD changes in TMD can reasonably be interpreted as part of a multimodal pain-regulation network rather than as isolated motor co-activation [19, 20].

The pattern observed in our results is consistent with this interpretation. The splint condition was associated with broader but fragmented cerebellar recruitment, CR by more spatially consolidated activation with the highest peak response, and CO by a more spatially restricted but statistically stronger average signal. At the same time, the generalized linear model did not demonstrate a robust global main effect of condition; instead, the dominant pattern was ROI-specific redistribution. This distinction is important. In light of recent cerebellar pain models, the present findings suggest that experimentally defined mandibular states may modulate the internal organization of cerebellar pain-related processing rather than shift cerebellar globally in a single direction. In other words, local cerebellar reweighting may be more informative than whole-structure averages in TMD [19, 20].

Broader evidence from musculoskeletal pain disorders also supports this interpretation. A 2023 meta-analysis of voxel-based morphometric studies identified decreased gray matter in the left cerebellum, alongside abnormalities in affective and cognitive pain-related regions [21]. A 2022 diffusion tensor imaging study demonstrated widespread white-matter alterations, supporting the idea that chronic musculoskeletal pain is accompanied by central microstructural reorganization [22].

Similarly, newer work in chronic low back pain has described disrupted cerebellar connectivity with large-scale cortical systems, including salience, emotional, and locus coeruleus-related pathways. [23] Taken together, these findings indicate that chronic musculoskeletal pain is better understood as a heterogeneous network disorder in which cerebellar involvement may be recurrent but phenotype-dependent rather than disease-specific.

This case therefore extends the current TMD neuroimaging literature in two ways. First, it brings the cerebellum to the foreground, whereas most recent TMD studies have focused on cortical, limbic, or graph-

theoretical whole-brain findings. Second, it demonstrates within-subject state dependence across mandibular conditions, suggesting that cerebellar responses may vary dynamically with occlusal-functional context. These observations should not be interpreted as evidence of therapeutic efficacy of any mandibular intervention. Rather, they support the view that cerebellar reactivity in TMD may be condition-sensitive and region-specific, with potential relevance for future mechanism-oriented and diagnostic neuroimaging studies.

The limitations of this report are inherent to its single-case design. The findings cannot establish causality, cannot be generalized to all patients with TMD, and should be regarded as hypothesis-generating. Nevertheless, the convergence between the present ROI-specific cerebellar results and the broader literature on pain neuroimaging suggests that the cerebellum deserves more explicit attention in future multimodal TMD studies, especially those combining TMJ MRI, task-based or resting-state fMRI, and cerebellar parcellation methods.

Abbreviations

AI
Activation index
BOLD
Blood oxygen level-dependent
CO
Centric occlusion
CR
Centric relation
FDR
False discovery rate
fMRI
Functional magnetic resonance imaging
GLM
General linear model
GRF
Gaussian random field
MRI
Magnetic resonance imaging
TMD
Temporomandibular disorder
ROI
Region of interest
SUIT
Spatially unbiased infratentorial template
VBM

Voxel-based morphometry

Declarations

Funding statement: This research did not receive any specific grant from funding agencies in the public, commercial, or not-for-profit sectors.

Conflict of interests: The authors declare that they have no competing interests.

Ethics approval: Written informed consent for publication and imaging analysis was obtained from the patient. This case report was prepared in accordance with institutional ethical requirements and the Declaration of Helsinki and was approved by the Commission on Ethics and Academic Integrity of the Shupyk National Healthcare University of Ukraine, Kyiv, Ukraine (Protocol No. 13/10, dated 17 December 2024). The data owner, the National Specialized Children's Hospital "OHMATDYT," Ministry of Health of Ukraine, Kyiv, Ukraine. Ukrainian Research Registration No. 0125U003930.

Author Contributions:

N.S. Validation; Writing - review and editing; Supervision, Investigation.

V.P. Conceptualization; Methodology; Formal analysis; Resources; Visualization; Writing - original draft, Validation.

I.R. Data curation; Software.

Availability of data and materials: De-identified data supporting the findings of this study are not publicly available due to the risk of re-identification and institutional restrictions but are available from the corresponding author on reasonable request and with permission of the data owner (National Specialized Children's Hospital "OHMATDYT", Kyiv, Ukraine).

Declaration of generative AI and AI-assisted technologies in the manuscript preparation process.

During the preparation of this work the authors used the following AI-assisted tools: Cursor (Anysphere Inc.; version 1.0) and ChatGPT (OpenAI; version 5.2) for writing and refining MATLAB code used for statistical data processing and visualization (including correlation analyses, group comparisons, and figure generation). All AI-generated code and text were reviewed, modified where necessary, and validated by the authors. The authors take full responsibility for the content of the published article and for the correctness of the analyses performed.

Corresponding author

Vasil Pekhno

PhD., Doctoral student, Department of Therapeutic and Pediatric Dentistry,

associate professor Department of Orthopedic Dentistry, Digital technologies and implantology, Shupyk National Healthcare University of Ukraine 9 Dorohozhytska Str., Kyiv, 04112 Ukraine

e-mail: *pekhnyo@ukr.net*

References

1. Jimsheleishvili S, Dididze M, Neuroanatomy. Cerebellum. In: StatPearls [Internet]. Treasure Island (FL): StatPearls Publishing; 2025 Jan– [updated 2023; cited 2026 Mar 20]. Available from: https://www.ncbi.nlm.nih.gov/books/NBK538167/
2. Manto M, Bower JM, Conforto AB, Delgado-García JM, da Guarda SNF, Gerwig M, et al. Consensus paper: roles of the cerebellum in motor control-the diversity of ideas on cerebellar involvement in movement. Cerebellum. 2012;11(2):457–87.
3. Borsook D, Moulton EA, Schmidt KF, Becerra LR. Human cerebellar responses to brush and heat stimuli in healthy and neuropathic pain subjects. Cerebellum. 2008;7(3):252–72.
4. Moulton EA, Schmahmann JD, Becerra L, Borsook D. The cerebellum and pain: passive integrator or active participator? Brain Res Rev. 2010;65(1):14–27.
5. Saab CY, Willis WD. The cerebellum: organization, functions and its role in nociception. Brain Res Brain Res Rev. 2003;42(1):85–95.
6. Apkarian AV, Bushnell MC, Treede RD, Zubieta JK. Human brain mechanisms of pain perception and regulation in health and disease. Eur J Pain. 2005;9(4):463–84.
7. Coombes SA, Misra G. Pain and motor processing in the human cerebellum. Pain. 2016;157(1):117–27.
8. Lickteig R, Lotze M, Kordass B. Successful therapy for temporomandibular pain alters anterior insula and cerebellar representations of occlusion. Cephalalgia. 2013;33(15):1248–57.
9. He SS, Li F, Gu T, Liu Y, Zou SJ, Huang XQ, et al. Altered neural activation pattern during teeth clenching in temporomandibular disorders. Oral Dis. 2016;22(5):406–14. 10.1111/odi.12465.
10. Tramonti Fantozzi MP, Diciotti S, Tessa C, Castagna B, Chiesa D, Barresi M, et al. Unbalanced occlusion modifies the pattern of brain activity during execution of a finger to thumb motor task. Front Neurosci. 2019;13:499. 10.3389/fnins.2019.00499.
11. Sato F, Tsutsumi Y, Oka A, Furuta T, Sohn J, Oi Y, et al. Projections from regions of the cerebellar nuclei receiving jaw muscle proprioceptive signals to trigeminal motoneurons and their premotoneurons in the rat pons and medulla. Cerebellum. 2025;24(4):113. 10.1007/s12311-025-01862-7.
12. Cho SY, Shin AS, Na BJ, Jahng GH, Park SU, Jung WS, et al. Brain activity associated with memory and cognitive function during jaw-tapping movement in healthy subjects using functional magnetic resonance imaging. Chin J Integr Med. 2013;19(6):409–17. 10.1007/s11655-012-1187-7.
13. Kobayashi T, Fukami H, Ishikawa E, Shibata K, Kubota M, Kondo H, et al. An fMRI study of the brain network involved in teeth tapping in elderly adults. Front Aging Neurosci. 2020;12:32. 10.3389/fnagi.2020.00032.

14. Nettekoven C, Diedrichsen J. Cerebellar asymmetries. Handb Clin Neurol. 2025;208:369–78. 10.1016/B978-0-443-15646-5.00005-1.
15. Yin Y, He S, Xu J, You W, Li Q, Long J, et al. The neuro-pathophysiology of temporomandibular disorders-related pain: a systematic review of structural and functional MRI studies. J Headache Pain. 2020;21(1):78. 10.1186/s10194-020-01131-4.
16. Shrivastava M, Ye L. Neuroimaging and artificial intelligence for assessment of chronic painful temporomandibular disorders: a comprehensive review. Int J Oral Sci. 2023;15(1):58. 10.1038/s41368-023-00254-z.
17. Li X, Jiang Y, Chen Z. Altered grey matter volume and cerebral perfusion over the whole brain in painful temporomandibular disorders: a pilot voxel-based analysis. Curr Med Imaging. 2025;21:e15734056373583. 10.2174/0115734056373583250531004637.
18. Jiang Y, Li X, Liu M, Chen Z. Investigating changes of functional brain networks in painful temporomandibular disorders: a resting-state fMRI study. J Oral Facial Pain Headache. 2026;40(1):61–70. 10.22514/jofph.2026.006.
19. Li CN, Keay KA, Henderson LA, Mychasiuk R. Re-examining the mysterious role of the cerebellum in pain. J Neurosci. 2024;44(17):e1538232024. 10.1523/JNEUROSCI.1538-23.2024.
20. Manda O, Hadjivassiliou M, Varrassi G, Zavridis P, Zis P. Exploring the role of the cerebellum in pain perception: a narrative review. Pain Ther. 2025;14(3):803–16. 10.1007/s40122-025-00724-8.
21. Xin M, Qu Y, Peng X, Zhu D, Cheng S. A systematic review and meta-analysis of voxel-based morphometric studies of fibromyalgia. Front Neurosci. 2023;17:1164145. 10.3389/fnins.2023.1164145.
22. Cheng S, Dong X, Zhou J, et al. Alterations of the white matter in patients with knee osteoarthritis: a diffusion tensor imaging study with tract-based spatial statistics. Front Neurol. 2022;13:835050. 10.3389/fneur.2022.835050.
23. Hall M, Dobson F, Klyne DM, Zheng CJ, Lima YL, Egorova-Brumley N. Neurobiology of osteoarthritis: a systematic review and activation likelihood estimation meta-analysis. Sci Rep. 2023;13(1):12442. 10.1038/s41598-023-39245-9.

Figures

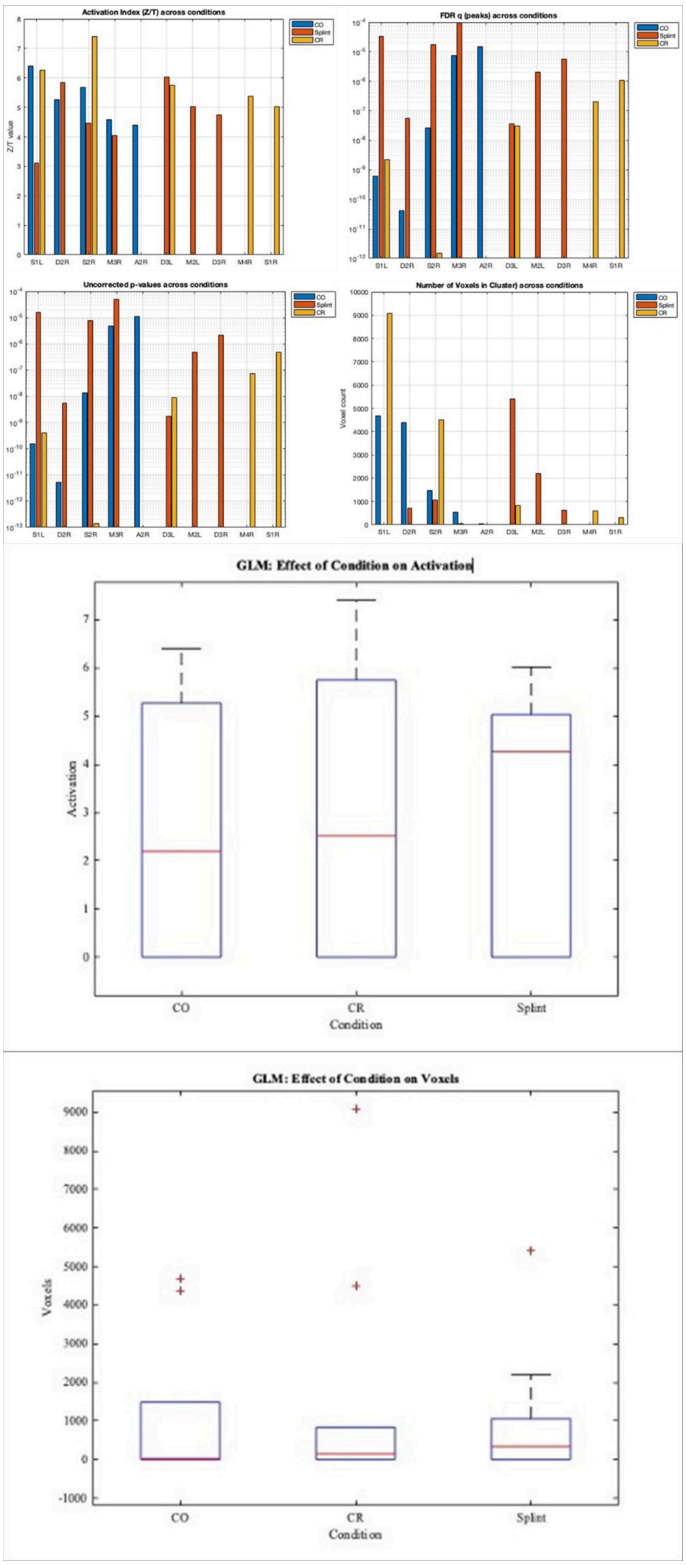


Figure 1

Legend not included with this version

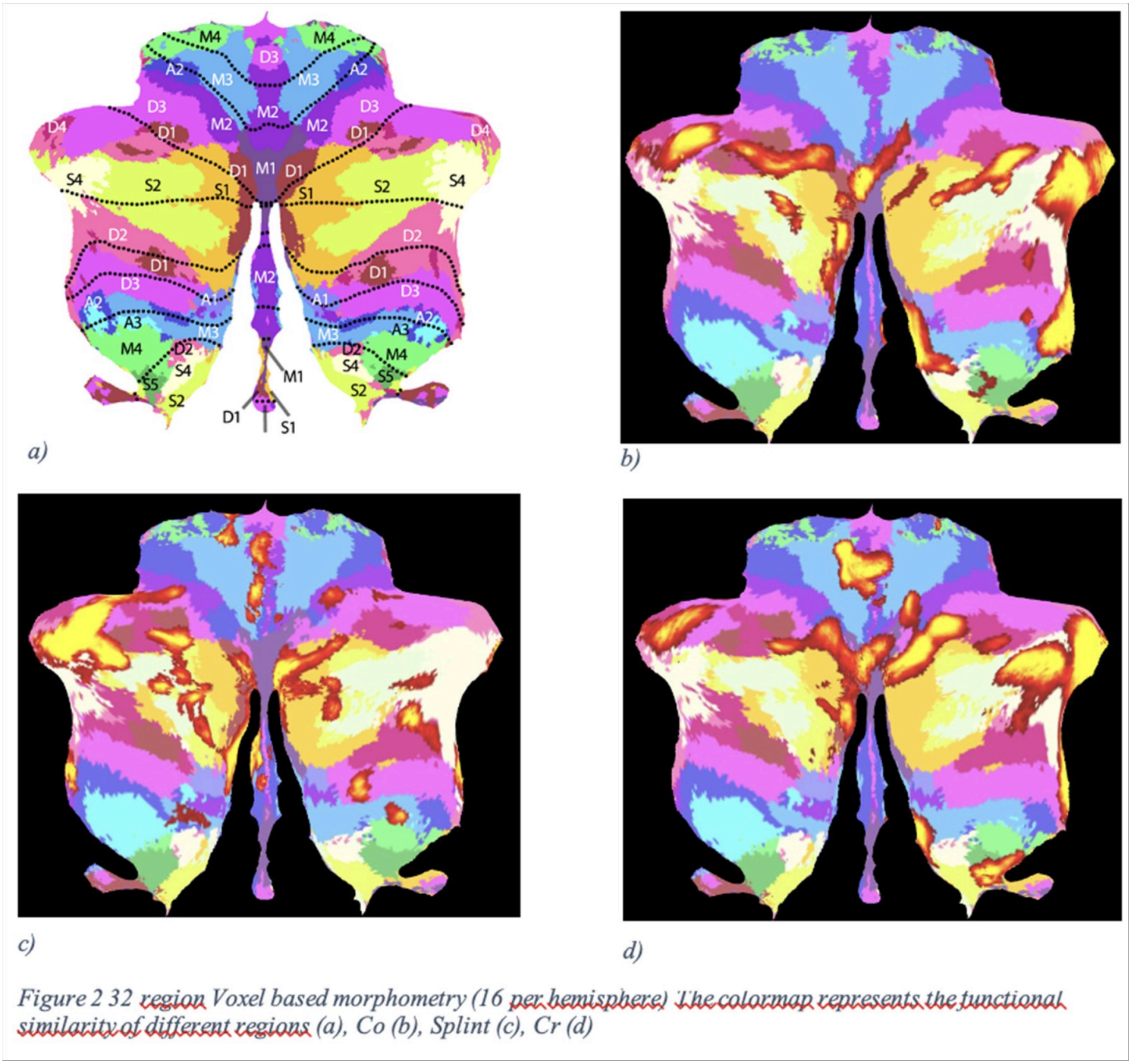


Figure 2 32 region Voxel based morphometry (16 per hemisphere) The colormap represents the functional similarity of different regions (a), Co (b), Splint (c), Cr (d)

Figure 2

See image above for figure legend

Supplementary Files

This is a list of supplementary files associated with this preprint. Click to download.

- CAREChecklist.docx